Photochemical CO_2 reduction using structurally controlled g-C_3N_4

James J. Walsh,[a] Chaoran Jiang,[b] Junwang Tang[b] and Alexander J. Cowan[a]*

[a.] *Stephenson Institute for Renewable Energy, University of Liverpool, L69 7ZF, Liverpool, UK. Email: a.j.cowan@liv.ac.uk*
[b.] *Solar Energy Group, Department of Chemical Engineering, University College London, Torrington Place, London, WC1E 7JE, UK.*

Electronic supplementary information

1 Experimental

Synthesis and materials: The three types of g-C_3N_4 were synthesised according to our previously published method.[S1] g-C_3N_4 was synthesised by thermal condensation of different organic precursors (urea, thiourea and dicyandiamide (DCDA)). Typically, a lidded alumina crucible with half the volume occupied by the precursor was placed inside a muffle furnace and heated at 600°C with a ramp rate of 5°C/min for 4 hours. The resultant powders were washed with deionised water and dried in air at 70°C for several hours before use.

CH_3CN (spec grade, Aldrich), triethanolamine (TEOA, Aldrich), 2,2'-bipyridine (bpy, Aldrich) and $CoCl_2.6H_2O$ (Aldrich) were used as purchased. Milli-Q water was used in all experiments. CO_2 (BOC) was CP grade.

Methods: The reaction suspension (consisting of g-C_3N_4 in 3:1:1 CH_3CN/H_2O/TEOA) was made up in a glass vial and sonicated for 10 minutes to ensure dispersion of the solid g-C_3N_4. The reactor used for photocatalysis was a 1 x 2 cm quartz cuvette (Starna) equipped with a B24 neck adaptor. The reaction suspension was added to this flask with a magnetic stirring bar neck was sealed with a rubber septum and purged with CO_2 for 20 minutes. The reaction mixture containing aqueous-soluble Co^{2+} and organic-soluble bpy phases was stirred vigorously throughout the experiment to prevent phase separation.[S2, S3] Samples for gas chromatography were taken at time zero and at intervals of one hour thereafter.

External quantum yield (EQE) measurements were conducted under LED or monochromated lamp illumination measured for each individual experiment. Optimisation of photocatalytic activity was performed using a 150 W Xe lamp equipped with a KG1 filter under constant power irradiation. Control experiments under argon, in the dark, and in the absence of either g-C_3N_4, TEOA, Co^{2+} or bpy showed minimal or no CO evolution (Table 1). Wavelength-dependent photocatalysis was conducted using a series of LEDs from LEDEngin purchased from RS Electronics: LZ1-00U600 (365 nm), LZ4-00UA00 (400 nm) LED or LZ1-00B200 (465 nm). The 420 nm LED (EPILED) were purchased from Amazon. Each LED was mounted onto a heat sink and driven using banana plugs and a power supply (TTI).

Gas product yields (dihydrogen and carbon monoxide) were quantified using an Agilent 6890N gas chromatograph employing N6 helium as the carrier gas (5 ml.min^{-1}). A 5 Å molecular sieve column (ValcoPLOT, 30 m length, 0.53 mm ID) and a pulsed discharge detector (D-3-I-HP, Valco Vici) were employed. CO and H_2 peak areas were quantified with multiple calibrant gas injections and were re-calibrated daily. ^{1}H-NMR spectroscopy of the post-reaction solution, to test for liquid CO_2 reduction products such as formic acid, was not possible due to the presence of paramagnetic Co^{2+}.

Inductively-coupled plasma mass spectrometry (ICP-MS) was performed using a dissolved g-C_3N_4 colloidal sol.[S4] Three photocatalytic experiments were setup using 365 nm LED at 5 mW/cm^2 for 2 hours. After the reaction, the solid g-C_3N_4 was centrifuged and washed with Milli-Q water. This process was repeated a further two times using clean water. The solid g-C_3N_4 (2.5 mg) was then dissolved in 5 ml of concentrated HNO_3 and refluxed at 80°C for 3 hours. After approximately one hour the cloudy suspension turned clear. The slightly yellow colloidal solution was cooled to room temperature and was stable over a period of several months, with no obvious precipitation. The UV/Vis spectra of the colloids revealed a delaminated solution and correlated well with the literature.[S4] Three post-reaction colloidal solutions were examined for Co content and the averaged data showed good reproducibility.

UV/Vis diffuse reflectance spectroscopy was performed using a Shimadzu 2600 spectrometer equipped with an integrating sphere using either 1 cm quartz cuvettes (suspensions) or glass microscope slides (solids).

Steady-state luminescence measurements were collected using a Perkin Elmer Fluorescence Spectrometer LS55 with slit widths of 10 nm and 2.5 nm at a scan rate of 500 nm/min. Spectra were recorded using suspensions of g-C_3N_4 in 1 x 1 cm

quartz cuvettes fitted with a B24 neck (Starna) and rubber septa. Samples were made by weighing out 1.0 mg g-C_3N_4 into 5 ml H_2O followed by 30 minutes sonication. The samples were then diluted 1:1 with CH_3CN containing bpy to give a final suspension of 0.1 mg/ml g-C_3N_4. Small aliquots (5-25 µl) of a concentrated (mM) Co^{2+} aqueous stock solution were titrated into the cuvette and the sample was purged with N_2 for 20 minutes before recording the spectrum. The excitation wavelength was chosen for each g-C_3N_4 type at a wavelength independent of absorbance changes upon addition of Co^{2+}.

Time-resolved luminescence measurements were recorded using a modified transient absorption setup employing the third harmonic of a Q-switched Nd:YAG laser (Continuum Minilite). Samples of g-C_3N_4 were compressed into solid discs for reflectance measurements using a die press either alone (DCDA, thiourea) or by mixing with an inert additive (urea, which did not form quality pellets without adding an additive such as NaCl). The samples were placed into a 1 x 2 cm quartz cuvette (Starna) fitted with a B24 neck, stoppered and purged with Ar for 20 minutes prior to excitation. The instrument response function (IRF) was recorded using $BaSO_4$. The time response was recorded using 355 nm laser excitation at 0.4 Hz and averaged over 500 shots. The reflected signal was focused through a monochromator and a bandpass filter (455 nm) to the detector. Data were recorded using a Si photodiode and preamplifier (MCA-200Hz) coupled to an oscilloscope (Tektronix TDS 2014C 100 MHz) and a computer running LabVIEW 2011, and were analysed using the deconvolution functions in Decayfit v 1.3 (Fluortools).

Transient absorption spectra were recorded using a diffuse reflectance sampling mode. Briefly, part of the output from a 75 W Xe lamp (OBB/PTi) was focused through a ND 50 % filter and onto the powdered sample held in a 1 mm quartz cuvette. All samples were thoroughly purged with argon (20 minutes) prior to use. The size of the probe beam was *ca.* 5 mm ∅ at the sample. Diffusely scattered light was collected using 1" plano-convex lens (Thor labs, UV grade silica) and directed through a monochromator (OBB/PTi) and a photodiode (Hamamatsu) coupled to a home-made preamplifier. The time resolution of the system (*ca.* 5 µs) was determined by the photodiode response and the amplification stages employed. Samples were excited using a Nd:YAG laser (Continuum Minilite) at 3 Hz, 355 nm, *ca.* 6 ns. The laser pulse was passed through a UV grade diffuser (Thor labs) to ensure that the entire sample is excited by the laser pulse. Experimental data were averaged for typically 100-250 laser shots. The transient data are presented in the manner previously employed in diffuse reflectance TA spectroscopy by Furube *et al*., where % absorption = (1 - R/R_0) x 100 where R and R_0 are the probe light intensities with and without excitation respectively.[S5] Wavelength-dependent transient data were acquired by adjusting the monochromator settings and recording an averaged kinetic trace every 50 nm.

FTIR spectra were collected using a Bruker Vertex spectrometer operating in transmittance mode. FTIR analysis of isotopically labelled products was performed using a custom built FTIR gas cell. The cell was comprised of plastic tube sealed at each end with 2 mm thick CaF_2 windows (Crystran) and Loctite Hysol epoxy resin (3422 A + B). A 1 cm diameter hole was drilled into the top of the cell and sealed with a fresh septum for each experiment, and the edge of the septum was sealed with silicone gel. The cell, which was *ca*. 2 cm in diameter and *ca*. 10 cm in length, was clamped horizontally in the beam path. Spectra were recorded using air as the background, for 128 scans, at a resolution of 0.5 cm^{-1}. Catalysis was performed using a 365 nm LED for 2 hours using $^{13}CO_2$ as the substrate. After the reaction, 5 ml of gas from the cell headspace were injected into our custom made cell and the spectrum acquired.

2 Optimization of photocatalytic conditions

Parameter						CO (µmol.h^{-1}.g^{-1})
g-C_3N_4	Light[a]	CO_2[b]	bpy	Co^{2+}	TEOA[c]	
Urea	✓	✓	✓	✓	✓	460
×	✓	✓	✓	✓	✓	< 0.01
✓	×	✓	✓	✓	✓	< 0.01
✓	✓	×	✓	✓	✓	0.01
✓	✓	✓	×	✓	✓	< 0.01
✓	✓	✓	✓	×	✓	< 0.01
✓	✓	✓	✓	✓	×	< 0.01

Table S1: Control experiments showing that photocatalysis depends on all factors being present. Conditions: 0.5 mg g-C_3N_4 per ml in CH_3CN/TEOA/H_2O (3:1:1), t = 2 h. a: KG1 illumination (see Fig. S3, λ = 300 – 795 nm with % T ≥ 10, 29 mW.cm^{-2}), b: Purged with Ar, c: Solvent mixture was 3:1 CH_3CN/H_2O.

In addition to the types of g-C_3N_4 screened (shown in Table 1, main paper), the ratios of bpy:Co^{2+} and the quantity of g-C_3N_4 per experiment were both tested over a range of values. An optimum ratio of 100 bpy per Co^{2+} was observed, in-line with studies using other types of g-C_3N_4 and *in-situ* formed $[Co(bpy)_n]^{2+}$.[S6]

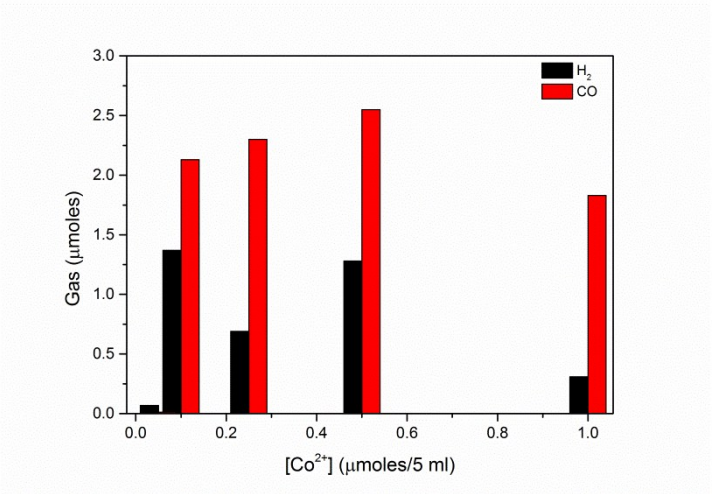

Fig. S1: Varying $[Co^{2+}]$ concentration at constant [bpy] and g-C_3N_4 *loading. Conditions: 0.5 mg g-C_3N_4 per ml in $CH_3CN/TEOA/H_2O$ (3:1:1), t = 2 h, under KG1 illumination (see Fig. S3, λ = 300 – 795 nm with % T ≥ 10, 29 mW.cm^{-2}).*

The relative photocatalytic efficiencies were then tested using the most efficient type of g-C_3N_4 (urea, data in Table 1) at optimised co-catalyst loading (100:1 bpy/Co^{2+}, data in Fig. S1). This was achieved by changing the loading of suspended g-C_3N_4. These data, shown in Fig. S2, revealed that a g-C_3N_4 concentration 2.5 mg/5 ml yielded the best photocatalytic response. This is likely the g-C_3N_4 loading with an optimum light absorption profile, neither too dilute nor too scattering.

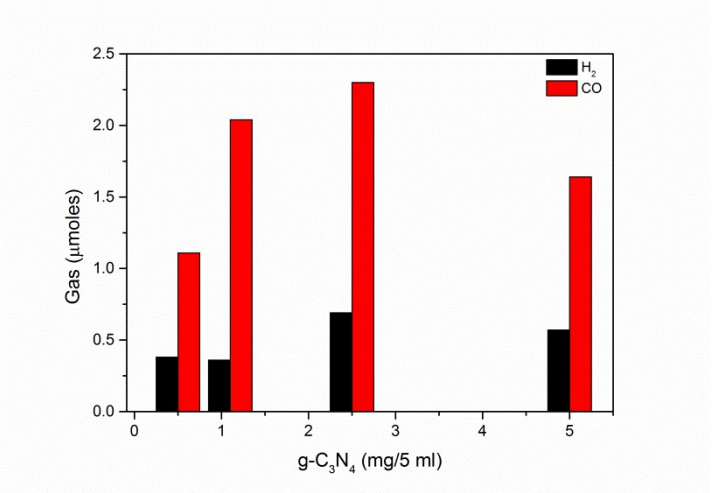

Fig. S2: Comparison of product yields using different quantities of g-C_3N_4 (urea) and constant concentrations of $[Co(bpy)_n]^{2+}$. Conditions: 0.5 mg g-C_3N_4 per ml in $CH_3CN/TEOA/H_2O$ (3:1:1), t = 2 h, under KG1 illumination (see Fig. S3, λ = 300 – 795 nm with % T ≥ 10, 29 mW.cm^{-2}).

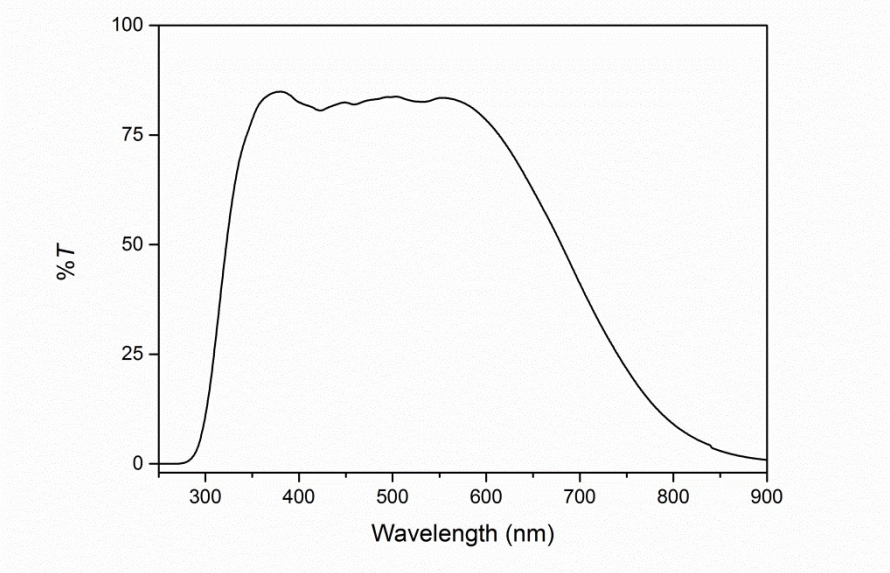

Fig. S3: Transmittance of KG1 filter used in Table 1, Fig. S1 and Fig. S2.

3 LED profiles and AQY measurements

The data in Fig. 1 (b), plotted overlaid with the diffuse-reflectance (DR) UV/Vis spectrum of g-C_3N_4 (urea), show that the photocatalytic activity drops off at 420 nm, in line with the reduced absorptivity of g-C_3N_4 (urea) at this wavelength, and by 465 nm the activity had dropped to zero. The photocatalytic activity is given as apparent quantum yield (% AQY) as calculated using Eq. S1:[S7]

$$\% AQY = \left[\frac{(2.n_{CO}.N_A.h.c)}{(t_{irr}.I.\lambda.A)}\right]100 \qquad \text{(S1)}$$

Where n_{CO} is moles of CO photogenerated; N_A is Avogadro's constant (6.022 x 10^{23} mol^{-1}); h is Planck's constant (6.626 x 10^{-34} J.s); c is the speed of light (3 x 10^8 $m.s^{-1}$); t_{irr} is the irradiation time; I and λ are the incident intensity ($W.cm^{-2}$) and wavelength of light (nm), respectively; and A is the irradiated area of the cell (cm^2).

4 Spectroscopy

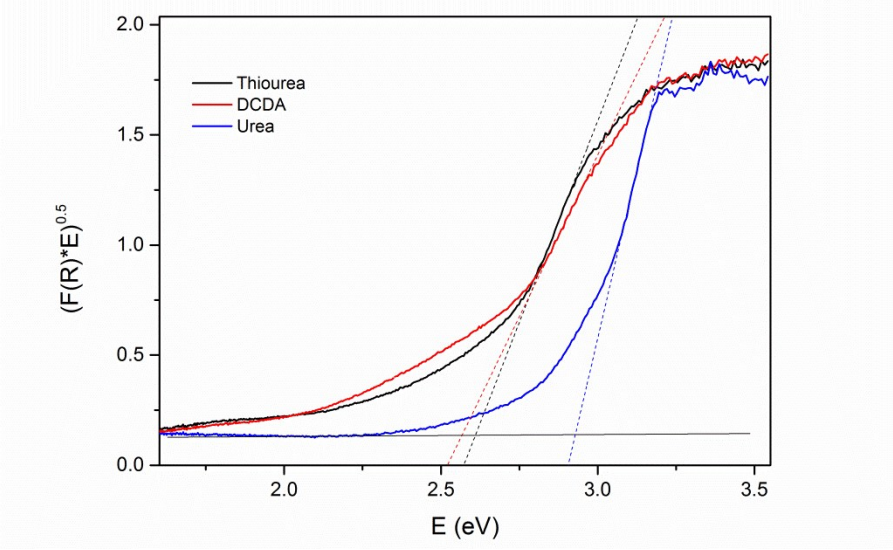

Fig. S4: Tauc plot of g-C_3N_4 derived from the precursors indicted.

Equation	y = a + b*x		
		Value	Standard Error
DCDA	Intercept	1	--
	Slope	17009.58162	63.80002
Urea	Intercept	1	--
	Slope	26252.12814	1275.53042
Thiourea	Intercept	1	--
	Slope	9262.82082	115.37089

Table S2: Fitting data for Stern-Volmer plots in Fig. 2. Data points and error bars are the mean and standard deviation of data from two independent datasets.

The data in Fig. 2 were plotted using the Stern-Volmer equation (Eq. S2):

$$\frac{I_0}{I} = 1 + K_{SV}[Q] \qquad \text{(S2)}$$

Where I and I_0 are the emission intensities of the quenched and unquenched fluorophores, respectively; [Q] is the concentration of Co^{2+} quencher and K_{SV} is the Stern-Volmer constant (Eq. S3):

$$K_{SV} = k_q.\tau_0 \qquad \text{(S3)}$$

From the SV plots it is possible to obtain a quenching rate constant; however care should be taken as the lack of linearity at higher concentrations may indicate the presence of inaccessible emissive sites[S8] and the emission decay kinetics of g-C_3N_4 are also shown to be multi-exponential complicating such analyses. Measurements of the photoluminescent lifetimes using a 355 nm Nd:YAG laser (5-6 ns FWHM) show that the three types of g-C_3N_4 all display lifetimes of similar length and all considerably longer than the IRF (Fig. S5). While the true lifetime values of each g-C_3N_4 type are difficult to measure accurately with our apparatus, we can draw two firm conclusions. Firstly the lifetimes of all three g-C_3N_4 agree very closely, and secondly the lifetimes do not exceed 10 ns. The similarities in τ_0 permit us to estimate relative k_q values for each g-C_3N_4 type, with g-C_3N_4 showing the highest relative k_q. Values for k_q are on the order of 10^{12} s^{-1}, which exceeds the diffusion controlled limit, implying a static quenching mechanism. Indeed, ICP-MS analysis of post-reaction g-C_3N_4 (urea) colloids[S4] revealed the presence of 44 ± 6 ppb Co, in contrast to < 1 ppb for g-C_3N_4 not used in photocatalysis. This corresponds to approximately 3.7 nmol of deposited Co^{2+}, meaning that *ca*. 1.5 molar % of Co^{2+} is deposited throughout a typical reaction (2 hours photocatalysis with 365 nm LED at 5 mW/cm^2). Photodeposition of Co^{2+} onto g-C_3N_4 has been observed previously.[S9, S10] While the photoluminescence experiments were performed under non-catalytic conditions (*i.e.*: in the absence of both CO_2 and TEOA), the ability of Co^{2+} to deposit on g-C_3N_4 can potentially provide a pathway for static quenching and explain the high k_q values obtained. Static quenching has been observed previously for g-C_3N_4 used as a photoluminescent sensor for metallic dications in solution, such as Hg^{2+},[S11] while mixed static/dynamic quenching has been observed for g-C_3N_4 quenching by Cu^{2+}.[S12]

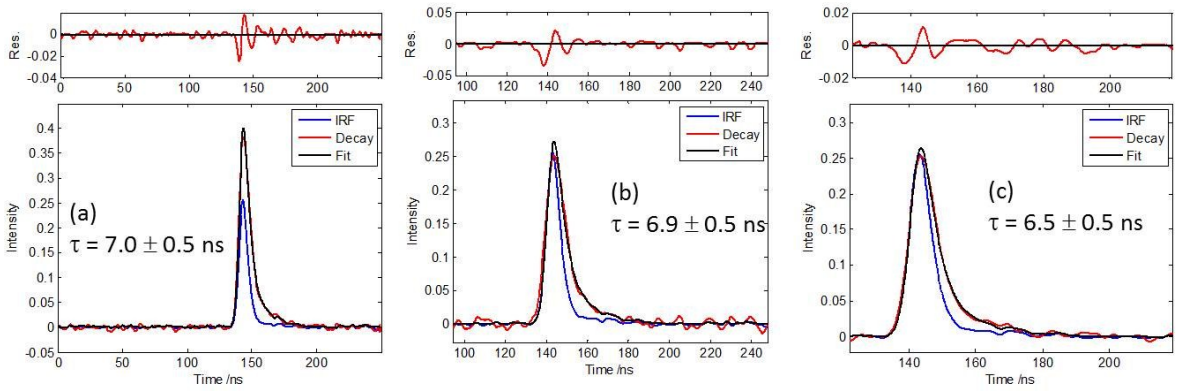

Fig. S5: Time-resolved emission decays monitored at 455 nm following 355 nm excitation of urea (a) thiourea (b) and DCDA (c) derived g-C_3N_4. The IRF is measured using a $BaSO_4$ standard. The lifetimes should be viewed as an approximate value given the similarity between the IRF and the decay functions. Data was fitted using the DecayFit v1.3 software by Fluortools (www.fluortools.com).

Wavelength dependent DR-TA spectra have been normalised for OD response over the range studied.

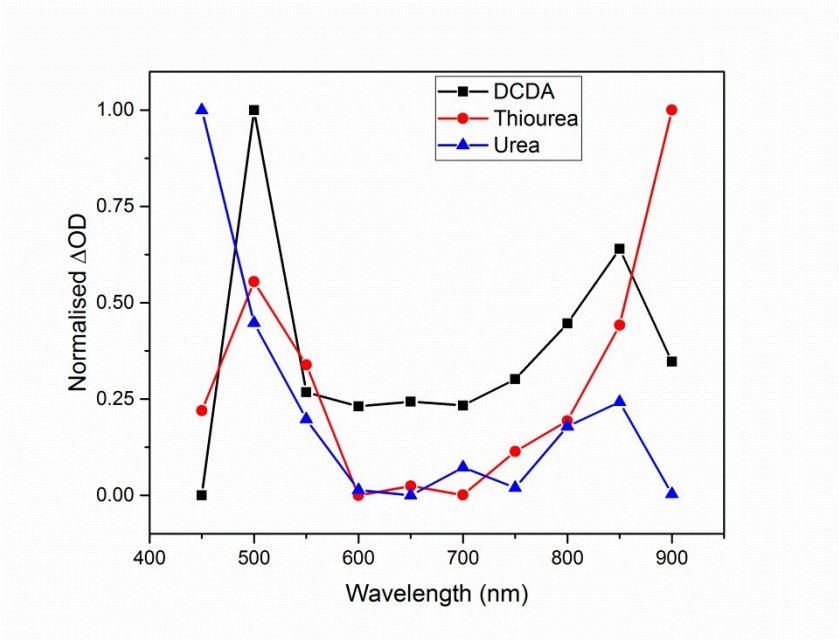

Fig. S6: Diffuse reflectance transient absorption spectra (normalised) 100 μs after laser pulse excitation.

The FTIR spectrum of the products formed from an experiment using $^{13}CO_2$ is shown in Fig. S7. The spectrum shows the presence of the ^{13}CO product with branches centred at 2075 and 2130 cm^{-1}, in line with the literature spectrum for ^{13}CO.[S13] The rising baseline at longer wavelengths is due to the presence of a very large $^{13}CO_2$ absorption. There is no detectable trace of ^{12}CO. The feature centred at 2017 cm^{-1} is due to the $^{13}CO_2$ substrate.

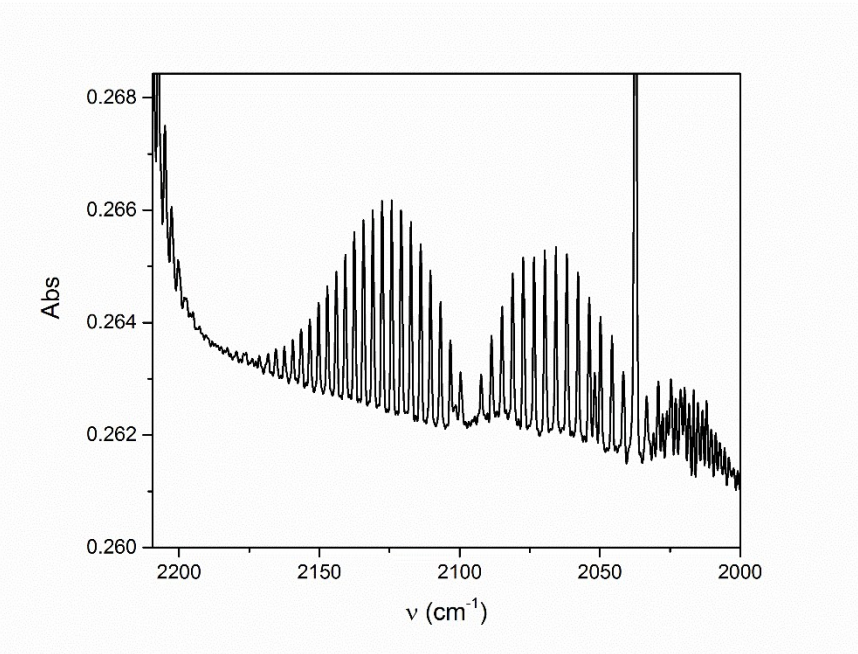

Fig. S7: FTIR spectrum of cell headspace of a $^{13}CO_2$ purged sample post-photocatalysis at 365 nm. The presence of ^{13}CO confirms that CO_2 is the carbon source for the CO production.

5 References

S1 D. J. Martin, K. Qiu, S. A. Shevlin, A. D. Handoko, X. Chen, Z. Guo and J. Tang, *Angew. Chem. Int. Ed.*, 2014, **53**, 9240–9245.

S2 J.-M. Lehn and R. Ziessel, *Proc. Natl. Acad. Sci. USA*, 1982, **79**, 701–704.

S3 R. Ziessel, J. Hawecker and J.-M. Lehn, *Helv. Chim. Acta*, 1986, **69**, 1065–1084.

S4 J. Zhang, M. Zhang, L. Lin and X. Wang, *Angew. Chem. Int. Ed.*, 2015, **54**, 6297–6301.

S5 A. Furube, Z.-S. Wang, K. Sunahara, K. Hara, R. Katoh and M. Tachiya, *J. Am. Chem. Soc.*, 2010, **132**, 6614–6615.

S6 J. Lin, Z. Pan and X. Wang, *ACS Sustain. Chem. Eng.*, 2014, **2**, 353–358.

S7 C. A. Caputo, M. A. Gross, V. W. Lau, C. Cavazza, B. V. Lotsch and E. Reisner, *Angew. Chem. Int. Ed.*, 2014, **53**, 11538–11542.

S8 J. R. Lakowicz, *Principles of Fluorescence Spectroscopy Principles of Fluorescence Spectroscopy*, 3rd ed., 2006, p 289.

S9 R.-L. Lee, P. D. Tran, S. S. Pramana, S. Y. Chiam, Y. Ren, S. Meng, L. H. Wong and J. Barber, *Catal. Sci. Technol.*, 2013, **3**, 1694–1698.

S10 L. Ge, C. Han, X. Xiao and L. Guo, *Appl. Catal. B Environ.*, 2013, **142-143**, 414–422.

S11 S. Barman and M. Sadhukhan, *J. Mater. Chem.*, 2012, **22**, 21832–21837.

S12 N. Cheng, P. Jiang, Q. Liu, J. Tian, A. M. Asiri and X. Sun, *Analyst*, 2014, **139**, 5065–5068.

S13 J. Agarwal, T. W. Shaw, C. J. Stanton, G. F. Majetich, A. B. Bocarsly and H. F. Schaefer, *Angew. Chem. Int. Ed.*, 2014, **53**, 5152–5155.